CHEMISTRY OF MATERIALS

Article

pubs.acs.org/cm

Atomic Layer Deposition of Metal Fluorides Using HF−Pyridine as the Fluorine Precursor

Younghee Lee,[†] Huaxing Sun,[†] Matthias J. Young,[‡] and Steven M. George*[,†,§]

[†]Department of Chemistry and Biochemistry, [‡]Department of Chemical and Biological Engineering, and [§]Department of Mechanical Engineering, University of Colorado, Boulder, Colorado 80309, United States

Supporting Information

ABSTRACT: The atomic layer deposition (ALD) of a variety of metal fluorides including ZrF_4, MnF_2, HfF_4, MgF_2, and ZnF_2 was demonstrated using HF from a HF−pyridine solution. In situ quartz crystal microbalance (QCM) studies were utilized to examine the growth of these metal fluorides. ZrF_4 ALD using tetrakis(ethylmethylamido) zirconium and HF as the reactants was studied as a model system. The QCM measurements determined a mass gain per cycle (MGPC) of 35.5 ng/(cm^2 cycle) for ZrF_4 ALD at 150 °C. This MGPC was equivalent to a growth rate of 0.9 Å/cycle at 150 °C. MnF_2, HfF_4, MgF_2, ZnF_2, and additional ZrF_4 were also grown using bis(ethylcyclopentadienyl) manganese, tetrakis(dimethylamido) hafnium, bis(ethylcyclopentadienyl) magnesium, diethylzinc, and zirconium tetra-*tert*-butoxide as the metal precursors, respectively. The growth rates for MnF_2, HfF_4, MgF_2, ZnF_2, and ZrF_4 ALD were 0.4, 0.8, 0.4, 0.7, and 0.6 Å/cycle, respectively, at 150 °C. All of these metal fluoride ALD systems displayed self-limiting reactions. Ex situ measurements of the growth rates using X-ray reflectivity and spectroscopic ellipsometry analysis agreed with the in situ QCM measurements. Analysis of the QCM mass changes after the individual metal precursor and HF exposures quantified HF adsorption after the HF reaction. The ZrF_4 and HfF_4 films acted as strong Lewis acids and adsorbed an average of two HF per deposited MF_y species after the HF reaction. In contrast, the MnF_2, MgF_2, and ZnF_2 films all behaved as weak Lewis acids and did not adsorb HF after the HF reaction. The refractive indices of the metal fluoride films were in agreement with previous optical measurements. Most of the metal fluoride films were crystalline as measured by X-ray diffraction studies. The majority of the metal fluoride films also had high purity as established by X-ray photoelectron spectroscopy studies. This pathway for metal fluoride ALD using HF−pyridine as the fluorine precursor will be useful for many applications of metal fluoride films such as optical coatings in the ultraviolet wavelength region.

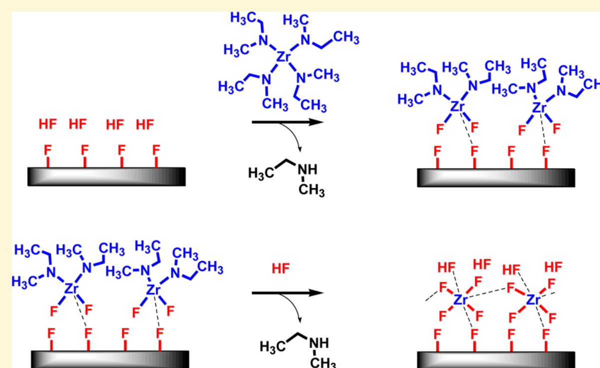

I. INTRODUCTION

Metal fluorides are important optical coating materials because they have a low refractive index and high transmission at ultraviolet (UV) and infrared (IR) wavelengths.[1−3] Some metal fluorides also have strong Lewis acidity and are used as heterogeneous catalysts for the manufacture of chlorofluorocarbons (CFCs).[4−6] Various metal fluorides, such as AlF_3, are also useful protective coatings on Li ion battery electrodes.[7,8] In addition, metal fluorides are known to be important surface reaction intermediates during thermal atomic layer etching (ALE).[9−11]

Metal fluoride films can be deposited using physical vapor deposition (PVD) methods. These PVD methods include sputtering,[12,13] thermal evaporation,[14−16] electron beam deposition,[1,17] and ion-assisted deposition.[18,19] Atomic layer deposition (ALD) methods can also be employed to grow metal fluorides. ALD is a technique that deposits extremely conformal and continuous thin films with atomic level control using sequential, self-limiting surface reactions.[20] In general, metal fluoride ALD has been difficult because the HF precursor is dangerous and corrosive. Consequently, the ALD of most metal fluorides has been performed using other fluorine precursors than HF.

The first demonstration of metal fluoride ALD reported CaF_2, SrF_2, and ZnF_2 ALD using NH_4F solid as the fluorine source.[21] NH_4F was delivered by sublimation at 80 °C into the reactor. The NH_4F decomposed to NH_3 and HF at reaction temperatures between 260 and 400 °C.[21] The ALD of MgF_2,[22,23] LaF_3,[24] YF_3,[25] and LiF[26] has been demonstrated using either TiF_4 or TaF_5 as the fluorine source. The ligand exchange between metal 2,2,6,6-tetramethyl-3,5-heptanedionate ($M(tmhd)_x$) and TiF_4 or TaF_5 yields the metal fluoride (MF_y) layer and volatile $Ti(tmhd)_4$ or $Ta(tmhd)_5$ as a byproduct. MgF_2 ALD has also been performed using anhydrous HF derived from a gas cylinder.[27] Hexafluoroacetylacetonate as the

Received: November 9, 2015
Revised: February 26, 2016
Published: March 1, 2016

 © 2016 American Chemical Society

DOI: 10.1021/acs.chemmater.5b04360
Chem. Mater. 2016, 28, 2022−2032

fluorine source together with ozone has also been used to grow MgF_2, CaF_2, and LaF_3 ALD films.[28]

We initially described AlF_3 ALD with trimethylaluminum (TMA) and HF from a HF−pyridine solution.[29,30] The HF−pyridine solution consists of 70% HF and 30% pyridine and is commonly referred to as Olah's reagent.[31] HF−pyridine is a liquid at room temperature and is in equilibrium with gaseous HF. Recent measurements have reported a HF vapor pressure of 90−100 Torr over HF−pyridine solutions.[10] Mass spectrometer experiments have also not detected measurable pyridine in the vapor above HF−pyridine solutions.[30] HF from HF−pyridine solutions avoids the problems of using HF from compressed gas cylinders and provides a safer alternative to anhydrous HF.

In this paper, the ALD of various metal fluorides was demonstrated using a variety of metal precursors and HF derived from HF−pyridine as the fluorine precursor. The metal precursors, tetrakis(ethylmethylamido) zirconium, bis(ethylcyclopentadienyl) manganese, tetrakis(dimethylamido) hafnium, bis(ethylcyclopentadienyl) magnesium, diethylzinc, and zirconium tetra-*tert*-butoxide, were employed for the ALD of ZrF_4, MnF_2, HfF_4, MgF_2, ZnF_2, and ZrF_4, respectively. The metal fluoride ALD was studied using in situ quartz crystal microbalance (QCM) investigations at 150 °C.

The thickness and density of metal fluoride ALD films were derived using ex situ X-ray reflectivity (XRR) analysis. In addition, the film thickness and refractive index of the metal fluorides were obtained using spectroscopic ellipsometry (SE). The composition and structure of the metal fluoride ALD films were also determined with X-ray photoelectron spectroscopy (XPS) and grazing incidence X-ray diffraction (GIXRD) analysis. These results should be useful for the growth and application of metal fluoride ALD films.

II. EXPERIMENTAL SECTION

II.I. Viscous Flow Reactor with in Situ QCM. The ALD reactions were conducted in a viscous flow reactor containing the in situ quartz crystal microbalance (QCM) at 150 °C.[32,33] A mechanical pump (Pascal 2015SD, Alcatel) provided vacuum conditions in the ALD reactor. The reactants were transported through the reactor using a N_2 carrier gas. Mass flow controllers (Type 1179A, MKS) delivered a constant N_2 carrier gas flow at 150 sccm. This N_2 gas flow and the pumping established a base pressure of ∼1 Torr in the reactor. The reactor was maintained at a fixed temperature within ±0.04 °C using a PID temperature controller (2604, Eurotherm). Pressure changes were monitored during the reactions using a bakeable capacitance manometer (Baratron 121A, MKS).

The metal fluoride ALD reactions were conducted using various metal precursors. These metal precursors were tetrakis(ethylmethylamido) zirconium (TEMAZ, 99.99%, Sigma-Aldrich,), bis(ethylcyclopentadienyl) manganese ($Mn(EtCp)_2$, 98%, Strem), tetrakis(dimethylamido) hafnium (TDMAH, 99.99%, Sigma-Aldrich), bis(ethylcyclopentadienyl) magnesium ($Mg(EtCp)_2$, 98%, Strem), diethylzinc (DEZ, Zn 52.0%, Sigma-Aldrich), and zirconium tetra-*tert*-butoxide (ZTB, 99%, Strem). The molecular structures of the various metal precursors are illustrated in Figure 1. The bubbler temperatures for TEMAZ, $Mn(EtCp)_2$, TDMAH, $Mg(EtCp)_2$, and ZTB were held at 112, 100, 67, 92, and 65 °C, respectively. The DEZ precursor was maintained at room temperature.

Each metal fluoride ALD experiment was performed on a fresh metal oxide ALD film that was grown at 150 °C. The initial metal oxide ALD films were prepared using the same metal precursors as employed for the metal fluoride ALD. H_2O (Chromasolv for HPLC, Sigma-Aldrich) was used as the reactant for the metal oxide ALD. HF−pyridine solution (70 wt % HF, Sigma-Aldrich) was contained in a gold-plated stainless steel bubbler and was transferred to this bubbler in a dry N_2-filled glovebag. The HF−pyridine and H_2O precursors were at room temperature.

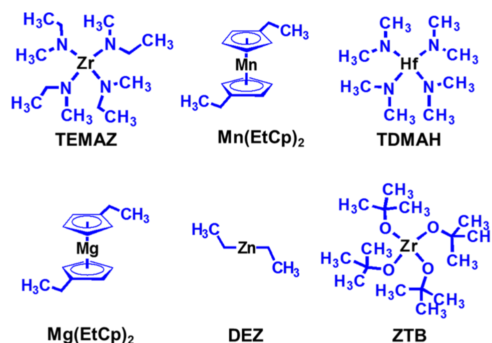

Figure 1. Molecular structures of various metal precursors. The CH_2 groups are not displayed explicitly.

The in situ QCM measurements were performed using a film deposition monitor (Maxtek TM-400, Inficon). The QCM sensors were 6 MHz, AT-cut (Colorado Crystal Corp.) quartz crystals that were polished and employed gold electrodes. The QCM sensor was contained in a bakeable single sensor head (BSH-150, Inficon). The QCM sensor was sealed with high-temperature epoxy (Epo-Tek H21D, Epoxy technology). To prevent deposition on the back-side of the QCM sensor, an additional 20 sccm of N_2 was flowed through the QCM housing.[32]

II.II. Ex Situ Film Characterization Using XRR, GIXRD, SE, and XPS. The substrates for the ex situ measurements were boron-doped Si(100) wafers (p-type, Silicon Valley Microelectronics). The Si wafer was cleaved to produce 2.5 cm by 2.5 cm samples. The sample cleaning procedure involved rinsing with acetone, isopropanol, and deionized water and then drying with N_2 gas.

Ex situ XRR measurements determined the film thicknesses and the density. A high-resolution X-ray diffractometer (Bede D1, Jordan Valley Semiconductors) using Cu Kα (λ = 1.540 Å) X-ray radiation was used for the XRR measurements. The step size and acquisition time for the XRR scans were 10 arcsec and 5 s, respectively. The Bede REFS software package (Bede REFS, Jordan Valley Semiconductors) was used to model the XRR scans to determine the film thickness, surface roughness, and film density. The same X-ray diffractometer was employed to study the film structure using GIXRD.

SE was used to obtain the film thicknesses and refractive indices. These measurements employed a spectroscopic ellipsometer (M-2000, J. A. Woollam) with a spectral range from 240−1700 nm and an incidence angle of 75°. The CompleteEASE software package (CompleteEASE, J. A. Woollam) and a Sellmier model were used to analyze the Ψ and Δ values.[34] The Sellmeier model is commonly used for optically transparent films such as metal fluoride films.[34]

XPS was used to determine the film composition.[30] The XPS instrument (PHI 5600) utilized a monochromatic Al Kα X-ray source (1486.6 eV). Depth profiles were obtained using Ar ion sputtering. The AugerScan software package (AugerScan, RBD Instruments) was employed to collect the data. The CasaXPS software package (CasaXPS, Casa Software) was used to analyze the data.

III. RESULTS AND DISCUSSION

III.I. ZrF_4 ALD Using Tetrakis(ethylmethylamido) zirconium (TEMAZ) and HF.

Figure 2, panel a shows the mass gain determined by QCM measurements during 200 cycles of ZrF_4 ALD at 150 °C using TEMAZ and HF. There was an initial layer of ZrO_2 on the QCM sensor grown with 200 cycles of ZrO ALD using TEMAZ and H_2O as the reactants.[35] The ZrF_4 ALD cycle was defined by a 1 s dose of TEMAZ, 40 s of N_2 purge, a 1 s dose of HF, and 40 s of N_2 purge. This reaction sequence is designated as (1−40−1−40). Pressure transients of 20 mTorr and 100 mTorr were produced by the TEMAZ and HF doses, respectively. The ZrF_4 ALD growth in

DOI: 10.1021/acs.chemmater.5b04360
Chem. Mater. 2016, 28, 2022−2032

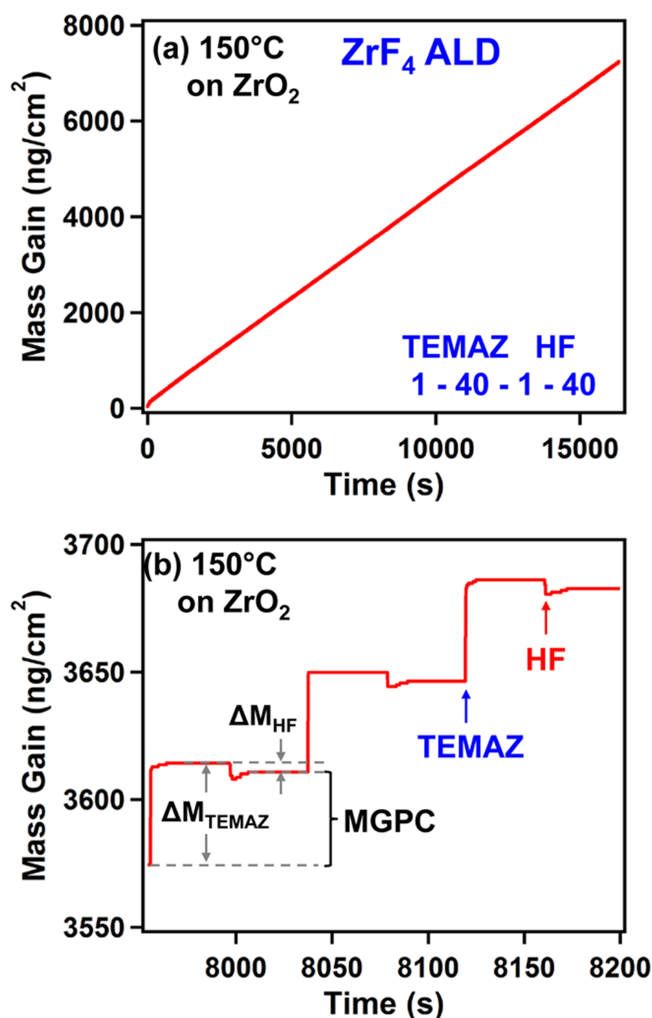

Figure 2. (a) Mass gain versus time during 200 ZrF_4 ALD cycles with TEMAZ and HF as the reactants on ZrO_2 at 150 °C using a reaction sequence of (1−40−1−40). (b) Enlargement of mass gain versus time for three sequential TEMAZ and HF exposures during ZrF_4 ALD in the steady-state, linear growth regime.

Figure 2, panel a is linear with a mass gain per cycle (MGPC) of 35.5 ng/(cm^2 cycle). In addition, ZrF_4 ALD experiments conducted on initial Al_2O_3 ALD films showed nearly identical results.

Figure 2, panel b displays the mass gain during three sequential ZrF_4 ALD cycles in the steady state region at 150 °C. These three cycles were the 98th, 99th, and 100th ZrF_4 ALD cycles in Figure 2, panel a. The mass changes coinciding with the reactant exposures are very distinct. The mass increase after the TEMAZ exposure is ΔM_{TEMAZ} = 39.2 ng/(cm^2 cycle). The mass change after the HF exposure is ΔM_{HF} = −3.7 ng/(cm^2 cycle). The MGPC is 35.5 ng/(cm^2 cycle).

Figure 3 shows the MGPC and the ΔM_{TEMAZ}/MGPC ratio during 200 cycles of ZrF_4 ALD. The MGPC is 35.5 ng/(cm^2 cycle) and consists of constant mass gains of ΔM_{TEMAZ} = 39.2 ng/(cm^2 cycle) and ΔM_{HF} = −3.7 ng/(cm^2 cycle). Except for the first three ZrF_4 ALD cycles, the ΔM_{TEMAZ}/MGPC ratio is constant at 1.1. The reaction stoichiometry will be determined later using this ratio. ZrF_4 ALD nucleates almost immediately on the initial ZrO_2 ALD surface. The MGPC and the ΔM_{TEMAZ}/MGPC ratio showed little dependence on the

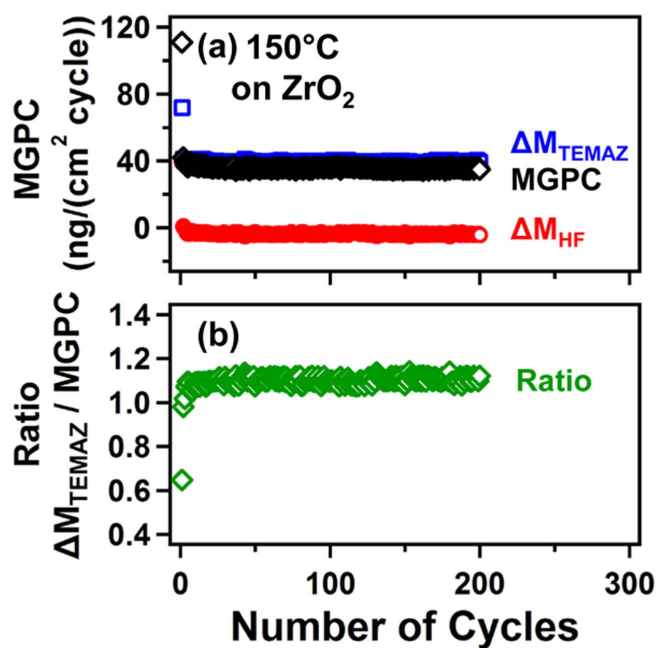

Figure 3. (a) MGPC, ΔM_{TEMAZ}, and ΔM_{HF} and (b) ΔM_{TEMAZ}/MGPC ratio during 200 ZrF_4 ALD cycles with TEMAZ and HF as the reactants on ZrO_2 at 150 °C.

purge time. The MGPC decreased slightly to ∼33 ng/(cm^2 cycle) after extended purge times of 120 s.

In situ QCM experiments also examined the self-limiting behavior of the TEMAZ and HF reactions. The mass gains during the TEMAZ and HF exposures at 150 °C are shown in Figure 4, panels a and b, respectively. The previous reactant exposure had reached saturation for each of these exposures. An

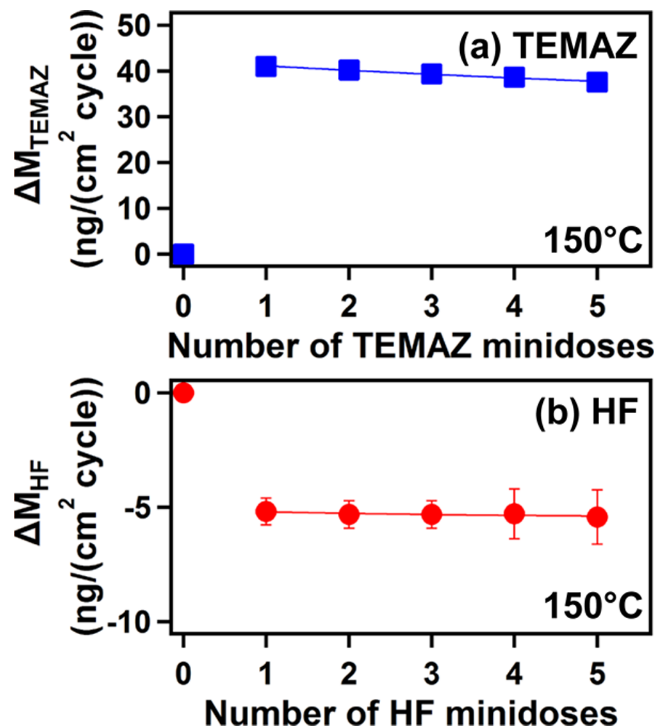

Figure 4. (a) ΔM_{TEMAZ} versus number of TEMAZ minidoses with the HF exposure fixed at 1.0 s. (b) ΔM_{HF} versus number of HF minidoses with the TEMAZ exposure fixed at 1.0 s.

DOI: 10.1021/acs.chemmater.5b04360
Chem. Mater. 2016, 28, 2022−2032

exposure time of 0.5 s and a purge time of 40 s defined each minidose. The TEMAZ and HF reactions both displayed self-limiting behavior. $\Delta M_{\mathrm{TEMAZ}}$ reached a plateau at $\Delta M_{\mathrm{TEMAZ}}$ = ~40 ng/(cm^2 cycle) after one minidose. Similarly, ΔM_{HF} leveled off at ΔM_{HF} = ~ −5 ng/(cm^2 cycle) after one minidose.

The film growth rate during ZrF_4 ALD was also determined from ex situ XRR and SE measurements. A ZrF_4 ALD film was grown on a Si wafer using 400 cycles of TEMAZ and HF reaction at 150 °C. XRR and SE measured the thickness of the ZrF_4 ALD film as 342 and 337 Å, respectively. These thicknesses are consistent with growth rates of 0.86 Å/cycle and 0.84 Å/cycle, respectively.

The MGPC of 35.5 ng/(cm^2 cycle) can be converted to a growth rate in Å/cycle using the film density. XRR measured a ZrF_4 film density of 4.1 g/cm^3. This XRR density of 4.1 g/cm^3 is ~93% of the bulk density of 4.43 g/cm^3 for crystalline ZrF_4.[36] This density can be used to convert the ZrF_4 ALD MGPC of 35.5 ng/(cm^2 cycle) to a growth rate of 0.87 Å/ cycle. There is good agreement between the in situ and ex situ measurements of the ZrF_4 ALD growth rate.

SE determined a refractive index of n = 1.55 at 589 nm for the ZrF_4 ALD films. The measured refractive index of n = 1.55 is consistent with previous measurements of n = 1.56 at 633 nm for amorphous ZrF_4,[37] n = 1.59 for crystalline ZrF_4,[37] and n = 1.62 for an e-beam grown ZrF_4 film at 600 nm.[1] The surface roughness of the ZrF_4 ALD films was measured as 4 Å by XRR. In addition, the ZrF_4 ALD films were stable in air. There was no change in the thickness, film density, and film roughness of the ZrF_4 films after exposure to atmosphere for one month.

III.II. Reaction Mechanism and Stoichiometry for ZrF_4 ALD. The surface chemistry for ZrF_4 ALD during the sequential TEMAZ and HF exposures can be defined by the following two reactions:

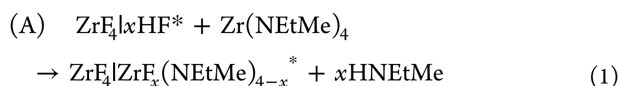

$$\text{(A)}\quad ZrF_4|xHF^* + Zr(NEtMe)_4 \rightarrow ZrF_4|ZrF_x(NEtMe)_{4-x}^* + xHNEtMe \tag{1}$$

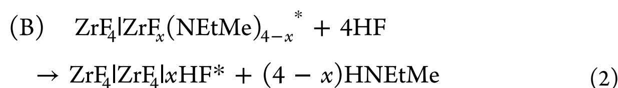

$$\text{(B)}\quad ZrF_4|ZrF_x(NEtMe)_{4-x}^* + 4HF \rightarrow ZrF_4|ZrF_4|xHF^* + (4-x)HNEtMe \tag{2}$$

The asterisks identify the surface species. The vertical lines separate the various surface species. HF converts $ZrF_x(NEtMe)_{4-x}$ to ZrF_4. HF can also adsorb on the ZrF_4 surface. The number of HF molecules adsorbed on the ZrF_4 surface relative to the number of ZrF_4 species deposited during one ZrF_4 ALD cycle is quantified by the parameter x.

Assuming this surface chemistry, the $\Delta M_{\mathrm{TEMAZ}}$/MGPC ratio can be established by

$$\frac{\Delta M_{\mathrm{TEMAZ}}}{\mathrm{MGPC}} = \frac{\Delta M_{\mathrm{TEMAZ}}}{\Delta M_{\mathrm{TEMAZ}} + \Delta M_{\mathrm{HF}}} = \frac{M_{\mathrm{TEMAZ}} - xM_{\mathrm{HNEtMe}}}{M_{\mathrm{ZrF4}}} \tag{3}$$

In eq 3, M_{TEMAZ}, M_{HF}, M_{NEtMe}, and M_{ZrF4} are the molar masses of TEMAZ, HF, HNEtMe, and ZrF_4, respectively. The equation for x is

$$x = \frac{1}{M_{\mathrm{HNEtMe}}}\left[M_{\mathrm{TEMAZ}} - M_{\mathrm{ZrF4}}\left(\frac{\Delta M_{\mathrm{TEMAZ}}}{\mathrm{MGPC}}\right)\right] = \frac{1}{59.1}\left[323.6 - 167.2\left(\frac{\Delta M_{\mathrm{TEMAZ}}}{\mathrm{MGPC}}\right)\right] \tag{4}$$

The QCM measurements at 150 °C shown in Figure 3, panel b yield a $\Delta M_{\mathrm{TEMAZ}}$/MGPC ratio of 1.1. This ratio of 1.1 produces x = 2.4 from eq 4. This x value of 2.4 indicates that there are 2.4 HF molecules adsorbed on the ZrF_4 surface after the HF exposure relative to each ZrF_4 species deposited during one ZrF_4 ALD cycle.

The proposed reaction mechanism for ZrF_4 ALD in the steady state regime using TEMAZ and HF as the reactants is shown in Figure 5. In reaction A, $Zr(NEtMe)_4$ molecules react

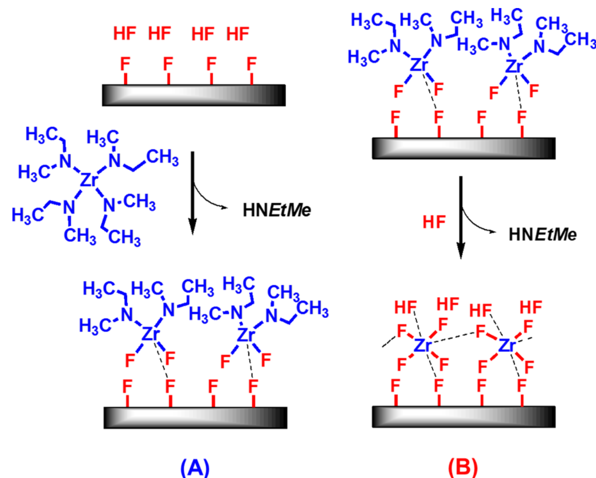

Figure 5. Proposed reaction mechanism for ZrF_4 ALD using TEMAZ and HF as the reactants.

with HF molecules adsorbed on the ZrF_4 surface to yield $ZrF_2(NEtMe)_2$ and HNEtMe as reaction products. Figure 5 shows two HF molecules per deposited ZrF_4 species during ZrF_4 ALD. The $ZrF_2(NEtMe)_2$ species remain adsorbed on the surface and HNEtMe is a volatile reaction product. In reaction B, HF converts the adsorbed $ZrF_2(NEtMe)_2$ species to ZrF_4. HNEtMe is again a volatile reaction product, and additional HF molecules adsorb to the ZrF_4 surface. The adsorption of HF on ZrF_4 is consistent with the strong Lewis acid nature of ZrF_4.[38]

III.III. MnF_2 ALD Using Bis(ethylcyclopentadienyl)-manganese ($Mn(EtCp)_2$) and HF. The QCM measurements of mass gain during 200 cycles of MnF_2 ALD at 150 °C using bis(ethylcyclopentadienyl) manganese ($Mn(EtCp)_2$) and HF are displayed in Figure 6, panel a. There was an initial layer of MnO on the QCM sensor grown with 200 cycles of MnO ALD using $Mn(EtCp)_2$ and H_2O as the reactants.[39] The reaction sequence was again (1−40−1−40). A nucleation period was observed over the first ~40 ALD cycles.

Figure 6, panel b displays the mass gain during three sequential MnF_2 ALD cycles in the steady state regime at 150 °C. These three cycles were the 98th, 99th, and 100th MnF_2 ALD cycles in Figure 6, panel a. Like the results shown in Figure 2, panel b for ZrF_4 ALD, the mass changes are very distinct. The mass increase after the $Mn(EtCp)_2$ exposure is $\Delta M_{\mathrm{Mn(EtCp)2}}$ = 40.8 ng/(cm^2 cycle). The mass loss after the HF exposure is ΔM_{HF} = −25.2 ng/(cm^2 cycle). The MGPC is 15.6

DOI: 10.1021/acs.chemmater.5b04360
Chem. Mater. 2016, 28, 2022−2032

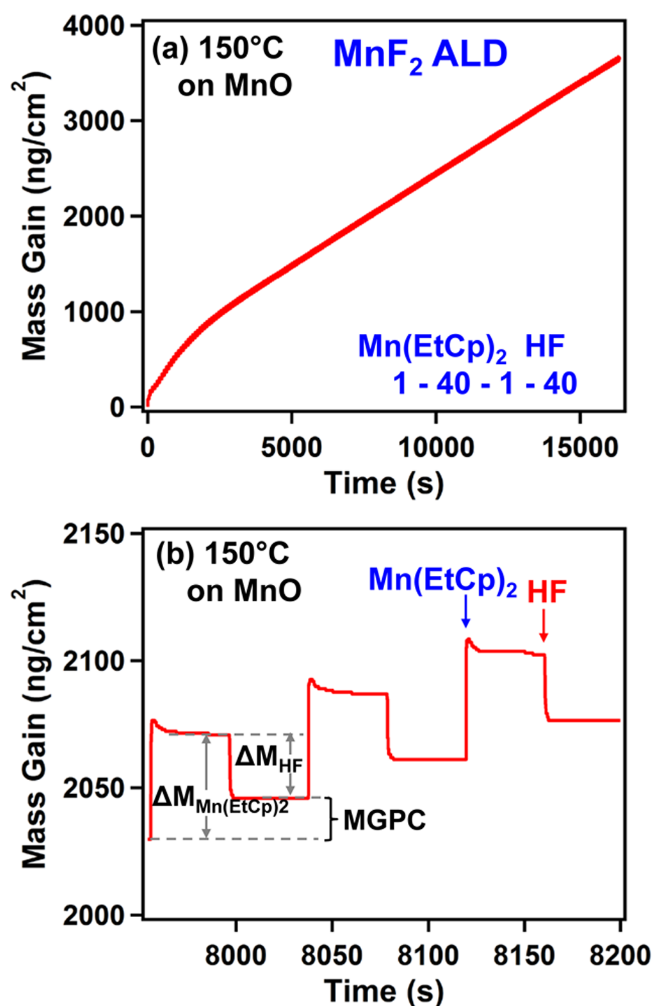

Figure 6. (a) Mass gain versus time during 200 MnF_2 ALD cycles with $Mn(EtCp)_2$ and HF as the reactants on MnO at 150 °C using the reaction sequence of (1−40−1−40). (b) Enlargement of mass gain versus time for three sequential $Mn(EtCp)_2$ and HF exposures during MnF_2 ALD in the steady-state, linear growth regime.

ng/(cm^2 cycle). The $\Delta M_{Mn(EtCp)2}$/MGPC ratio averaged from 100 to 200 cycles of MnF_2 ALD is 2.6.

The MnF_2 ALD growth rate was also derived from ex situ XRR and SE measurements. A MnF_2 film was grown on a Si wafer using 400 cycles of $Mn(EtCp)_2$ and HF reaction at 150 °C. XRR and SE analysis then measured MnF_2 film thicknesses of 172 and 179 Å, respectively. These thicknesses were consistent with growth rates of 0.43 Å/cycle and 0.45 Å/cycle. The XRR measurements obtained a MnF_2 density of 3.8 g/cm^3. This density is ~95% of the bulk density of 3.98 g/cm^3 for crystalline MnF_2.[36] This density can be used to convert the MnF_2 ALD MGPC of 15.6 ng/(cm^2 cycle) to a growth rate of 0.41 Å/cycle. This growth rate is in good agreement with the in situ QCM measurements.

The surface roughness of the MnF_2 ALD films was measured as 26 Å by XRR. This high surface roughness suggests that the MnF_2 ALD film is crystalline. SE determined a refractive index of n = 1.50 at 589 nm. This measured refractive index is consistent with the previously measured refractive index of n = 1.47−1.50 for MnF_2 at 589 nm.[34] The MnF_2 ALD films were also stable in air. Like the ZrF_4 ALD films, the thickness, film density, and film roughness of MnF_2 films were constant during storage for one month in atmosphere.

III.IV. Reaction Mechanism and Stoichiometry for MnF_2 ALD. The surface chemistry for MnF_2 ALD during the sequential $Mn(EtCp)_2$ and HF exposures can be expressed by these two reactions:

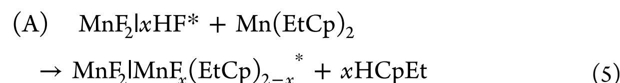

$$\text{(A)}\quad MnF_2|xHF^* + Mn(EtCp)_2 \rightarrow MnF_2|MnF_x(EtCp)_{2-x}^* + xHCpEt \qquad (5)$$

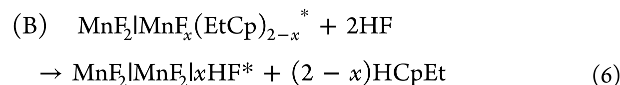

$$\text{(B)}\quad MnF_2|MnF_x(EtCp)_{2-x}^* + 2HF \rightarrow MnF_2|MnF_2|xHF^* + (2-x)HCpEt \qquad (6)$$

The asterisks again indicate the surface species and the vertical lines separate the different surface species. HF converts $MnF_x(EtCp)_{2-x}$ to MnF_2. HF can also adsorb on the MnF_2 surface. The number of HF molecules adsorbed on the MnF_2 surface relative to the number of MnF_2 species deposited during one MnF_2 ALD cycle is measured by the parameter x.

Given this surface chemistry for MnF_2 ALD, the $\Delta M_{Mn(EtCp)2}$/MGPC ratio can be derived from

$$\frac{\Delta M_{Mn(EtCp)2}}{MGPC} = \frac{\Delta M_{Mn(EtCp)2}}{\Delta M_{Mn(EtCp)2} + \Delta M_{HF}} = \frac{M_{Mn(EtCp)2} - xM_{HCpEt}}{M_{MnF2}} \qquad (7)$$

In eq 7, $M_{Mn(EtCp)2}$, M_{HF}, M_{HCpEt}, and M_{MnF2} are the molar masses of $Mn(EtCp)_2$, HF, HCpEt, and MnF_2, respectively. The equation for x is

$$x = \frac{1}{M_{HCpEt}}\left[M_{Mn(EtCp)2} - M_{MnF2}\left(\frac{\Delta M_{Mn(EtCp)2}}{MGPC}\right)\right] = \frac{1}{94.2}\left[241.2 - 92.9\left(\frac{\Delta M_{Mn(EtCp)2}}{MGPC}\right)\right] \qquad (8)$$

The QCM measurements at 150 °C yield a $\Delta M_{Mn(EtCp)2}$/MGPC ratio of 2.6. This ratio of 2.6 produces x = 0 from eq 8 and indicates that there are no HF molecules adsorbed on the surface relative to each MnF_2 species deposited during one MnF_2 ALD cycle. The lack of HF adsorption is in agreement with MnF_2 behaving as a weak Lewis acid with negligible interaction between HF and the MnF_2 film.

Figure 7 displays the proposed reaction mechanism for MnF_2 ALD in the steady state regime using $Mn(EtCp)_2$ and HF as the reactants. In reaction A, $Mn(EtCp)_2$ molecules are adsorbed on the MnF_2 surface. In reaction B, HF converts the adsorbed $Mn(EtCp)_2$ species to MnF_2 and HCpEt is a volatile reaction product. There are no HF molecules remaining on the MnF_2 surface after the HF exposure.

III.V. Growth of Additional Metal Fluoride ALD Films. HfF_4, MgF_2, ZnF_2, and additional ZrF_4 ALD films were also demonstrated using the appropriate metal precursor and HF as the reactants. In each case, the initial layer on the QCM sensor was grown using the metal precursor and H_2O as the reactants. The reaction sequence for all of the metal fluoride ALD systems, except ZnF_2 ALD, was (1−40−1−40). All the metal fluorides, except ZnF_2, showed similar nucleation on their corresponding metal oxides and on Al_2O_3 ALD films. The metal fluoride films were also stable in air. The thickness, film density, and film roughness of films were constant during

DOI: 10.1021/acs.chemmater.5b04360
Chem. Mater. 2016, 28, 2022−2032

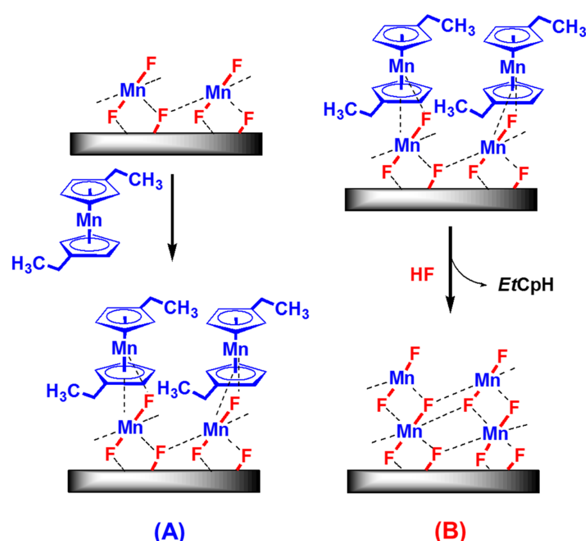

Figure 7. Proposed reaction mechanism for MnF_2 ALD using $Mn(EtCp)_2$ and HF as the reactants.

storage in atmosphere for one month. Only the ZnF_2 ALD film was stored in a desiccator until the ex situ measurements because of its instability in air. Measurements for ZnF_2 ALD are presented in the Supporting Information.

Figure 8 shows the QCM measurements of mass gain during 200 cycles of HfF_4, ZrF_4, and MgF_2 ALD at 150 °C. The initial layer on the QCM sensor was the corresponding metal oxide ALD film grown with 200 cycles of ALD using the metal precursor and H_2O as the reactants.[35,40,41] Figure 8 reveals that the ALD of these three metal fluorides is linear versus the sequential metal precursor and HF exposures except for a brief nucleation period over the first ∼10−12 ALD cycles for ZrF_4 and MgF_2 ALD.

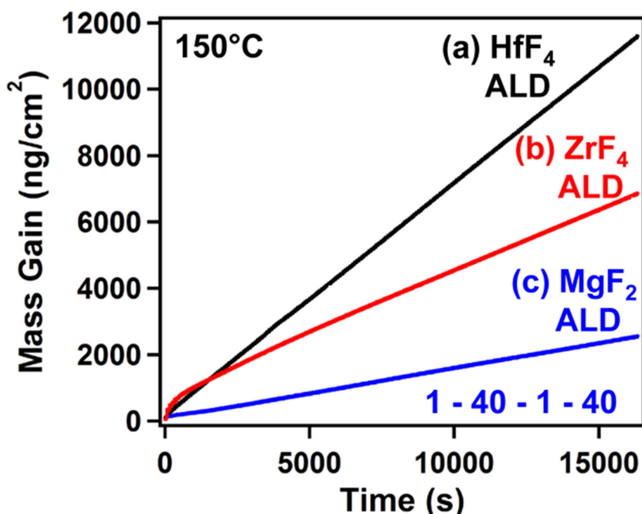

Figure 8. Mass gain versus time during 200 cycles of: (a) HfF_4 ALD; (b) ZrF_4 ALD; and (c) MgF_2 ALD at 150 °C using the reaction sequence of (1−40−1−40).

Figure 9 shows the mass gain during three sequential ALD cycles for HfF_4, ZrF_4, and MgF_2 ALD in the steady state regions at 150 °C. These three cycles were in the linear regimes of the ALD growth displayed in Figure 8. The mass gains are very distinct for each metal fluoride. The mass changes after the metal precursor and HF exposures are summarized in Table 1. The MGPCs are also given in Table 1. The mass change during the metal precursor exposure divided by the MGPC defines the ΔM_{TDMAH}/MGPC, ΔM_{ZTB}/MGPC, and $\Delta M_{Mg(EtCp)2}$/MGPC ratios. These ratios are also included in Table 1.

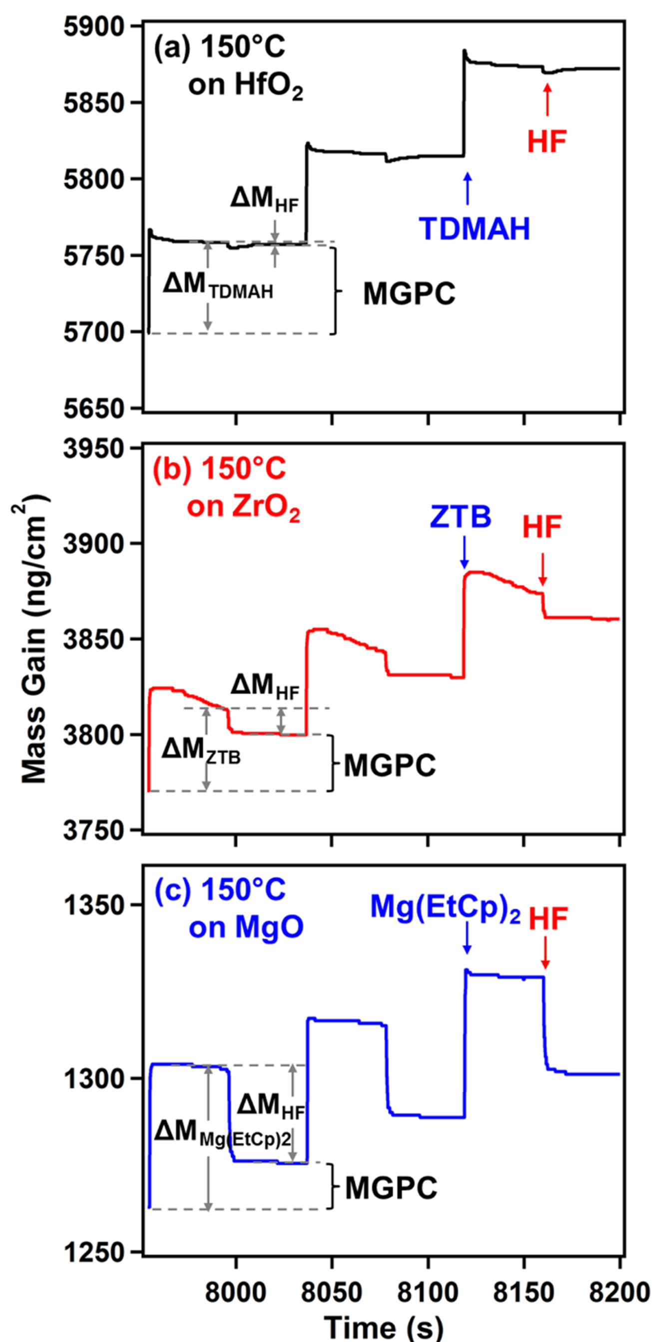

Figure 9. Enlargement of mass gain versus time for three sequential metal precursor and HF exposures in the steady-state, linear growth regime at 150 °C during: (a) HfF_4 ALD; (b) ZrF_4 ALD; and (c) MgF_2 ALD.

The ratios determine the x values that quantify the number of HF molecules adsorbed on the surface relative to the number of metal fluoride species deposited during one ALD cycle. By using similar equations as given by eqs 4 and 8 for ZrF_4 ALD and MnF_2 ALD, respectively, x values of 2.2, 2.0, and 0.1 can be determined for HfF_4, ZrF_4, and MgF_2 ALD, respectively. The x values of 2.2 and 2.0 indicate that there are 2.2 and 2.0 HF

DOI: 10.1021/acs.chemmater.5b04360
Chem. Mater. 2016, 28, 2022−2032

Table 1. Mass Changes, Growth Rates, Ratios, Number of HF per Metal Fluoride, and Lewis Acidity for the Various Metal Fluorides

metal fluoride	metal precursor (MP)	MGPC (ng/(cm^2 cycle))	ΔM_{MP} (ng/(cm^2 cycle))	ΔM_{HF} (ng/(cm^2 cycle))	growth rate at 150 °C (Å/cycle)	ratio	number of HF per MF_y	Lewis acidity
ZrF_4	TEMAZ	35.5	39.2	−3.7	0.9	1.1	2.4	strong
HfF_4	TDMAH	57.2	58.4	−1.2	0.8	1.0	2.2	strong
ZrF_4	ZTB	29.8	42.0	−12.2	0.6	1.4	2.0	strong
AlF_3	TMA	31.4	22.3	9.1	1.0	0.7	0.8	strong
MnF_2	$Mn(EtCp)_2$	15.6	40.8	−25.2	0.4	2.6	0	weak
MgF_2	$Mg(EtCp)_2$	12.3	39.5	−27.2	0.4	3.2	0.1	weak
ZnF_2	DEZ	33.5	41.4	−7.9	0.7	1.2	0	weak
LiF	LiHMDS	12.2	67.6	−55.4	0.5	5.6	0.1	Lewis base

molecules adsorbed on the HfF_4 and ZrF_4 surfaces, respectively, relative to each metal fluoride species deposited during one ALD cycle. This behavior is consistent with HfF_4 and ZrF_4 acting as strong Lewis acids. In contrast, the x value of 0.1 indicates that there is only 0.1 HF molecule adsorbed on the MgF_2 surface relative to each MgF_2 deposited during one MgF_2 ALD cycle. This behavior is in agreement with MgF_2 acting as a weak Lewis acid.

Metal fluoride ALD films were also grown on Si wafers using 400 cycles of metal precursor and HF at 150 °C. XRR and SE measurements of the film thicknesses are consistent with growth rates of 0.8, 0.6, and 0.4 Å/cycle for HfF_4, ZrF_4, and MgF_2 ALD, respectively. These growth rates are in good agreement with the growth rates determined by the MGPCs and film densities. The film densities determined from XRR analysis are summarized in Table 1. These densities are ∼96%, ∼106%, and ∼98% of the bulk densities of HfF_4, ZrF_4, and MgF_2.[36]

SE analysis also determined refractive indices of n = 1.55, n = 1.62, and n = 1.40 at 589 nm for the HfF_4, ZrF_4, and MgF_2 ALD films. The HfF_4 refractive index of n = 1.55 at 589 nm is in good agreement with previous measurements of n = 1.57 at 600 nm for e-beam evaporated HfF_4 film,[2] n = 1.59 at 600 nm for sputtered HfF_4 films,[42] and n = 1.62 at 600 nm for e-beam grown HfF_4 films.[1] The ZrF_4 refractive index of n = 1.62 at 589 nm is fairly consistent with n = 1.56 measured for amorphous ZrF_4 at 633 nm,[37] n = 1.59 for crystalline ZrF_4 at 600 nm,[37] and n = 1.62 at 600 nm for ZrF_4 films grown by e-beam evaporation.[1] The MgF_2 refractive index of n = 1.40 at 589 nm is consistent with refractive indices for MgF_2 of n = 1.37−1.38 at 589 nm[34] and n = 1.38 at 600 nm for MgF_2 films grown by sputtering.[42]

Surface roughnesses were also derived from the XRR analysis. The surface roughness of the HfF_4 ALD films was measured as 5 Å. The surface roughness of the ZrF_4 films was measured as 4 Å. The surface roughness of the MgF_2 films was measured as 12 Å. This larger surface roughness may result from a higher degree of crystallinity in the MgF_2 ALD film.

III.VI. Lewis Acid Strength of Metal Fluorides Based on HF Adsorption. Table 1 summarizes the growth rates, ratios, and x values for the various metal fluorides. The results for AlF_3 and LiF from other studies are also included in Table 1.[30,43] The x values give the number of HF molecules adsorbed on the surface relative to each MF_y species deposited during one MF_y ALD cycle. The x values divide the metal fluorides into two main groups. High x values of x = 2.0−2.4 are obtained for HfF_4 and ZrF_4. These surfaces act as strong Lewis acids and adsorb HF. Lower x values of $x \approx 0$ are obtained for MnF_2, MgF_2, and ZnF_2. These surfaces act as weak Lewis acids and do not adsorb HF.

This classification of metal fluorides into two categories based on their x values is consistent with the Lewis acid properties of the various metal fluorides. ZrF_4 and HfF_4 are both polymeric solids with eight-coordinate metal centers that are known to form the monoclinic crystal structure.[38,44] ZrF_4 and HfF_4 are known to display strong Lewis acid properties. Investigations of ZrF_4 and HfF_4 complexes with neutral O- and N-donor ligands have revealed that the large metal Zr and Hf centers can produce up to eight-coordination without difficulty.[38] A variety of ligands, such as dimethyl sulfoxide and 2,2′-bipyridyl, were also explored and shown to yield stable complexes with ZrF_4 and HfF_4. These complexes were consistent with the Zr and Hf centers acting as Lewis acids by accepting electron pairs from the ligands.[38]

HF is a fluorinating agent where the fluorine in HF acts as an anion. The Lewis acidity of ZrF_4 and HfF_4 can be viewed in terms of their ability to adsorb HF by interacting with the F^- anion. Evidence for F^- interaction with ZrF_4 is obtained from studies of molten salt chemistry. In molten salts, ZrF_4 forms the ZrF_6^{2-} anion by accepting two F^- anions by the reaction $ZrF_4 + 2F^- \rightarrow ZrF_6^{2-}$.[45] In addition, ZrF_4 is expected to be a Lewis acid because ZrO_2 is known to be an acidic oxide and acts as an oxide ion acceptor.[46] HfF_4 has also been categorized as a Lewis acid based on its facility to catalyze the isomerization of methylpentane to 2,2-dimethyl pentane and n-hexane and the simultaneous deprotonation of carbonium ion intermediates.[47,48]

In contrast, MnF_2, MgF_2, and ZnF_2 have lower values of $x \approx 0$ and do not adsorb HF. MnF_2, MgF_2, and ZnF_2 are all difluorides that form the rutile crystal structure. These difluorides are known to display weak Lewis acid properties. Infrared studies of CO adsorption on MgF_2 reveal the presence of medium or weak Lewis acid sites from magnesium atoms on the MgF_2 surface.[49] Pyrrole adsorption experiments also are consistent with the existence of weak basic sites from the fluorine atoms on the MgF_2 surface.[49] Similar infrared investigations of CO adsorption on ZnF_2 reveal that the Lewis acidity is even weaker at the Zn^{2+} sites on ZnF_2 surfaces compared with the Lewis acid sites on MgF_2 surfaces.[50]

The metals in MnF_2, MgF_2, and ZnF_2 have low electronegativities and are more likely to donate the F^- anion than accept the F^- anion. Viewed in terms of the metal oxides, MnO, MgO, and ZnO are all basic oxides and act as oxide ion donors.[46] The corresponding MnF_2, MgF_2, and ZnF_2 metal fluorides would be expected to act as F^- ion donors rather than F^- ion acceptors. The low Lewis acidity of MnF_2, MgF_2, and ZnF_2 leads to their negligible interaction with HF.

DOI: 10.1021/acs.chemmater.5b04360
Chem. Mater. 2016, 28, 2022−2032

The abilities of AlF_3 and LiF to adsorb HF are also consistent with their Lewis acid strengths. An x value of $x = 0.8$ was measured earlier during AlF_3 ALD studies.[30] This x value is consistent with the Lewis acid nature of AlF_3. AlF_3 can adsorb HF because AlF_3 can act as an F^- ion acceptor. Gaseous AlF_3 is a very strong Lewis acid.[51] Solid AlF_3 also has strong Lewis acid sites when AlF_3 is in the β-AlF_3 phase.[6,52,53] An x value of $x = 0.1$ was also measured during LiF ALD studies. This x value is consistent with the Lewis base nature of LiF.[54] LiF does not adsorb HF because LiF would rather act as a F^- ion donor.

III.VII. Ex Situ Film Characterization Using SE, XRD, and XPS. Figure 10 shows the refractive indices of the metal fluoride ALD films in the spectral range between 240 and 1700 nm. Figure 10 includes the refractive indices of AlF_3 and LiF. The refractive indices measured at 589 nm are summarized in Table 2. Most of these refractive indices are consistent with the bulk refractive indices reported in the literature as mentioned earlier. The refractive indices of $n = 1.55$ for the ZrF_4 ALD film and $n = 1.55$ for the HfF_4 ALD film were obtained using the TEMAZ and TDMAH precursors, respectively. ZrF_4 ALD films grown using the ZTB precursor have a higher refractive index $n = 1.62$ attributed to the ~10% oxygen impurity as discussed below.

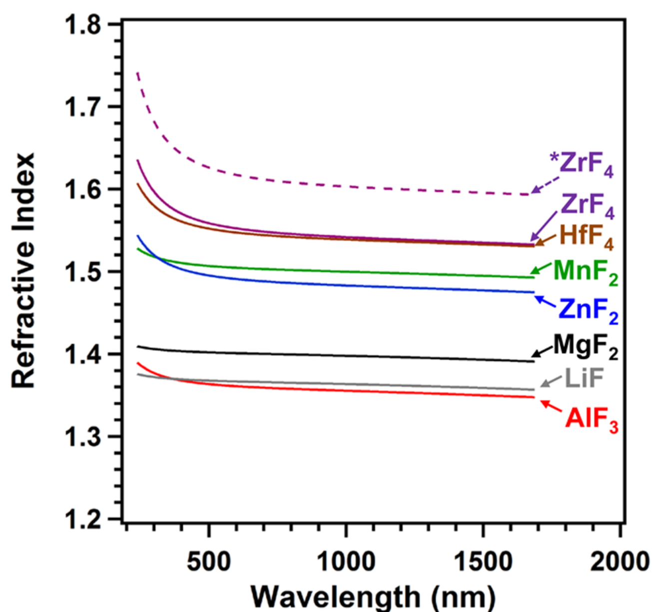

Figure 10. Refractive indices for metal fluoride ALD films grown at wavelengths between 240 and 1700 nm. These refractive indices were obtained from SE using the Sellmeier model.

GIXRD analysis indicated that most of the metal fluoride ALD films have crystalline structures. The metal fluorides yielding an amorphous film structure were ZnF_2 and AlF_3. The amorphous structure of ZrF_4 using ZTB as the precursor probably resulted from the oxygen impurity in the ZrF_4 film. ZrF_4 using TEMAZ as the precursor yielded a crystalline structure consistent with the monoclinic phase as given by the Joint Committee on Powder Diffraction Standards (JCPDS) file no. 33−1480. A broad peak at 23° with a full width at half-maximum (FWHM) of 7° corresponds to the overlap of the ZrF_4 $(\bar{1}21)$ and ZrF_4 $(\bar{2}11)$ peaks. Another broad peak at 50° was consistent with the ZrF_4 (024) peak.

HfF_4 using TEMAH as the precursor also displayed a crystalline structure consistent with the monoclinic phase (JCPDS # 79−1040). A very similar broad feature at 23° was observed that corresponded to the overlap of the HfF_4 (021) and HfF_4 (111) peaks. A broad HfF_4 $(\bar{5}31)$ peak was also observed at 50°. These broad peaks suggested that ZrF_4 and HfF_4 have nanocrystalline structure, which leads to wide diffraction peaks as predicted by the Scherrer equation.

MnF_2 film has a crystalline structure consistent with the tetragonal phase (JCPDS# 88−2143). The MnF_2 (110), MnF_2 (101), MnF_2 (211), and MnF_2 (220) peaks were located at 25.8°, 32.8°, 50.6°, and 53.2°, respectively. MgF_2 has a crystal structure consistent with the tetragonal phase (JCPDS# 72−2231). The MgF_2 (110), MgF_2 (111), MgF_2 (211), and MgF_2 (301) peaks were located at 27.5°, 40.7°, 53.5°, and 68.4°, respectively. The LiF film has a crystalline structure consistent with the cubic phase (JCPDS# 04−0857). The LiF (111), LiF (200), and LiF (220) peaks were located at 38.4°, 44.8°, and 65.3°, respectively. The crystalline structures of the metal fluoride films are summarized in Table 2.

XPS sputter depth-profiling revealed the impurity levels in the metal fluoride films. The XPS results indicate that most of the metal fluoride ALD films have very low levels of impurities. Sputter depth-profiles for the ZrF_4 and HfF_4 ALD films are shown in Figure 11, panels a and b, respectively. The ZrF_4 ALD film was deposited using TEMAZ as the metal precursor. After sputtering into the depth of the metal fluoride films, HfF_4 and

Table 2. Densities, Refractive Indices, Crystalline Structures, and Impurities for the Various Metal Fluorides. The JCPDS File Numbers Are Given for the Crystal Structures

metal fluoride	density (g/cm^3)	refractive index	crystal structure	impurities by XPS
ZrF_4 (TEMAZ)	4.1	1.55	monoclinic (33−1480)	1.1 at.% O, 3.4 at.% C
HfF_4	6.8	1.55	monoclinic (79−1040)	no O, C, or N
ZrF_4 (ZTB)	4.7	1.62	amorphous	10 at% O, no C
AlF_3	2.9	1.36	amorphous	2.1 at% O, no C
MnF_2	3.8	1.50	tetragonal (88−2143)	0.8 at% O, no C
MgF_2	3.1	1.40	tetragonal (72−2231)	1.0 at% O, no C
ZnF_2	4.9	1.49	amorphous	no O or C
LiF	2.6	1.37	cubic (04−0857)	no O, C, N, or Si

DOI: 10.1021/acs.chemmater.5b04360
Chem. Mater. 2016, 28, 2022−2032

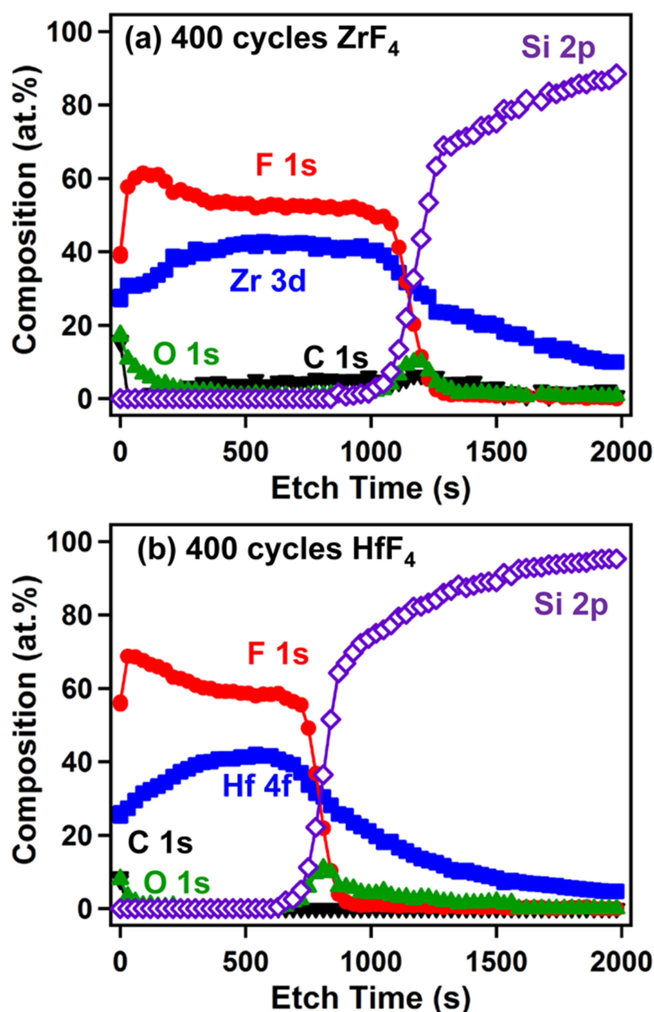

Figure 11. XPS sputter depth-profiles for (a) ZrF_4 ALD films grown using 400 ALD cycles with TEMAZ as the metal precursor and (b) HfF_4 ALD films grown using 400 ALD cycles with TDMAH as the metal precursor.

ZnF_2 had no detectable O or C impurities above the XPS detection limit of ~0.2 at.%. The MnF_2 and MgF_2 films had very low O impurities of ≤1.0 at.% and no measurable C impurities. The ZrF_4 film grown using TEMAZ had a larger C impurity of 3.4 at.% and a low O impurity of 1.1 at.%. The impurities in the metal fluoride ALD films are summarized in Table 2.

The ratios between the zirconium and fluorine XPS signals in Figure 11, panel a and the hafnium and fluorine XPS signals in Figure 11, panel b indicate fluorine deficiencies. Fluorine deficient metal fluorides have been observed previously in XPS studies of AlF_3 and LiF ALD films.[29,30,43] However, Rutherford backscattering spectra (RBS) have confirmed that the AlF_3 ALD films were stoichiometric even though the XPS results were showing fluorine deficiencies.[29,30] The preferential sputtering of fluorine may explain the low fluorine XPS signals.[18,19,30,55]

The higher levels of oxygen at the surface of the ZrF_4 film in Figure 11, panel a may indicate the interaction of the ZrF_4 film with moisture.[56] The ZrF_4 ALD film grown using ZTB as the metal precursor had a high O impurity level of ~10 at.%. This high oxygen impurity level is attributed to some incorporation of the alkoxide ligand from ZTB into the ZrF_4 ALD film. In contrast, the ZrF_4 ALD films grown using TEMAZ as the metal precursor had a lower O impurity of only 1.1 at.%.

IV. CONCLUSIONS

Various metal fluorides were grown using ALD techniques with HF−pyridine as the HF source. The metal fluorides were ZrF_4, MnF_2, HfF_4, MgF_2, and ZnF_2. The growth of these metal fluorides was monitored using in situ QCM measurements. ZrF_4 ALD using tetrakis(ethylmethylamido) zirconium and HF displayed a MGPC of 35.5 ng/(cm^2 cycle) at 150 °C. This MGPC was equivalent to growth rate of 0.9 Å/cycle. MnF_2, HfF_4, MgF_2, ZnF_2, and additional ZrF_4 were also grown and displayed growth rates of 0.4, 0.8, 0.4, 0.7, and 0.6 Å/cycle, respectively, at 150 °C. Nearly all of the ex situ measurements of the growth rates using XRR and SE analysis were in agreement with the in situ QCM measurements. All of these metal fluoride ALD systems displayed self-limiting reactions.

The mass changes measured by the QCM after the individual metal precursor and HF exposures were able to quantify HF adsorption on the metal fluoride surface after the HF reaction. The ZrF_4 and HfF_4 films adsorbed an average of two HF per deposited MF_y species after the HF reaction. This behavior is consistent with ZrF_4 and HfF_4 acting as strong Lewis acids. In comparison, the MnF_2, MgF_2, and ZnF_2 films did not adsorb HF after the HF reaction. This behavior is consistent with MnF_2, MgF_2, and ZnF_2 behaving as weak Lewis acids.

The metal fluoride ALD films displayed refractive indices that were consistent with previous measurements. XRD studies revealed that the majority of the metal fluorides were crystalline. XPS investigations showed that most of the metal fluorides had high purity. Metal fluoride ALD using HF−pyridine as the HF source will be useful for many applications of metal fluorides as optical films, protective coatings for Li ion battery electrodes and catalysts.

■ ASSOCIATED CONTENT

Ⓢ Supporting Information

The Supporting Information is available free of charge on the ACS Publications website at DOI: 10.1021/acs.chemmater.5b04360.

QCM measurements of ZnF_2 ALD using diethylzinc and HF; QCM, XRR, and SE measurements of growth rate for ZnF_2 ALD; surface roughness and refractive index of ZnF_2 ALD films (PDF)

■ AUTHOR INFORMATION

Corresponding Author

*E-mail: steven.george@colorado.edu.

Notes

The authors declare no competing financial interest.

■ ACKNOWLEDGMENTS

The National Science Foundation (CHE-1306131) funded this research. The Department of Energy through the DOE-BATT program provided additional personnel support for Y.L.

■ REFERENCES

(1) Pellicori, S. F.; Colton, E. Fluoride Compounds for IR Coatings. *Thin Solid Films* **1992**, *209*, 109−115.

(2) Traylor Kruschwitz, J. D.; Pawlewicz, W. T. Optical and Durability Properties of Infrared Transmitting Thin Films. *Appl. Opt.* **1997**, *36*, 2157−2159.

(3) Niisaka, S.; Saito, T.; Saito, J.; Tanaka, A.; Matsumoto, A.; Otani, M.; Biro, R.; Ouchi, C.; Hasegawa, M.; Suzuki, Y.; Sone, K. Development of Optical Coatings for 157-nm Lithography. I. Coating Materials. *Appl. Opt.* **2002**, *41*, 3242−3247.
(4) Herron, N.; Farneth, W. E. The Design and Synthesis of Heterogeneous Catalyst Systems. *Adv. Mater.* **1996**, *8*, 959−968.
(5) Kemnitz, E.; Gross, U.; Rudiger, S.; Shekar, C. S. Amorphous Metal Fluorides with Extraordinary High Surface Areas. *Angew. Chem., Int. Ed.* **2003**, *42*, 4251−4254.
(6) Kemnitz, E.; Menz, D. H. Fluorinated Metal Oxides and Metal Fluorides as Heterogeneous Catalysts. *Prog. Solid State Chem.* **1998**, *26*, 97−153.
(7) Ding, F.; Xu, W.; Choi, D. W.; Wang, W.; Li, X. L.; Engelhard, M. H.; Chen, X. L.; Yang, Z. G.; Zhang, J. G. Enhanced Performance of Graphite Anode Materials by AlF_3 Coating for Lithium-Ion Batteries. *J. Mater. Chem.* **2012**, *22*, 12745−12751.
(8) Sun, Y. K.; Lee, M. J.; Yoon, C. S.; Hassoun, J.; Amine, K.; Scrosati, B. The Role of AlF_3 Coatings in Improving Electrochemical Cycling of Li-Enriched Nickel-Manganese Oxide Electrodes for Li-Ion Batteries. *Adv. Mater.* **2012**, *24*, 1192−1196.
(9) Lee, Y.; DuMont, J. W.; George, S. M. Mechanism of Thermal Al_2O_3 Atomic Layer Etching Using Sequential Reactions with $Sn(acac)_2$ and HF. *Chem. Mater.* **2015**, *27*, 3648−3657.
(10) Lee, Y.; DuMont, J. W.; George, S. M. Atomic Layer Etching of HfO_2 Using Sequential, Self-Limiting Thermal Reactions with $Sn(acac)_2$ and HF. *ECS J. Solid State Sci. Technol.* **2015**, *4*, N5013−N5022.
(11) Lee, Y.; George, S. M. Atomic Layer Etching of Al_2O_3 Using Sequential, Self-Limiting Thermal Reactions with $Sn(acac)_2$ and Hydrogen Fluoride. *ACS Nano* **2015**, *9*, 2061−2070.
(12) Taki, Y. Film Structure and Optical Constants of Magnetron-Sputtered Fluoride Films for Deep Ultraviolet Lithography. *Vacuum* **2004**, *74*, 431−435.
(13) Iwahori, K.; Furuta, M.; Taki, Y.; Yamamura, T.; Tanaka, A. Optical Properties of Fluoride Thin Films Deposited by RF Magnetron Sputtering. *Appl. Opt.* **2006**, *45*, 4598−4602.
(14) Heitmann, W. Vacuum Evaporated Films of Aluminum Fluoride. *Thin Solid Films* **1970**, *5*, 61−67.
(15) Lee, C. C.; Liu, M. C.; Kaneko, M.; Nakahira, K.; Takano, Y. Characterization of AlF_3 Thin Films at 193 nm by Thermal Evaporation. *Appl. Opt.* **2005**, *44*, 7333−7338.
(16) Barriere, A. S.; Lachter, A. Optical Transitions in Disordered Thin Films of Ionic Compounds MgF_2 and AlF_3 as a Function of Their Conditions of Preparation. *Appl. Opt.* **1977**, *16*, 2865−2871.
(17) Bridou, F.; Cuniot-Ponsard, M.; Desvignes, J. M.; Richter, M.; Kroth, U.; Gottwald, A. Experimental Determination of Optical Constants of MgF_2 and AlF_3 Thin Films in the Vacuum Ultra-Violet Wavelength Region (60−124 nm), and its Application to Optical Designs. *Opt. Commun.* **2010**, *283*, 1351−1358.
(18) Schink, H.; Kolbe, J.; Zimmermann, F.; Ristau, D.; Welling, H. "Reactive Ion-Beam-Sputtering of Fluoride Coatings for the UV/VUV Range". *Proc. SPIE* **1990**, 327−338.
(19) Targove, J. D.; Bovard, B. G.; Lingg, L. J.; Angus Macleod, H. Densification of Aluminum Fluoride Thin-Films by Ion-Assisted Deposition. *Thin Solid Films* **1988**, *159*, L57−L59.
(20) George, S. M. Atomic Layer Deposition: An Overview. *Chem. Rev.* **2010**, *110*, 111−131.
(21) Ylilammi, M.; Rantaaho, T. Metal Fluoride Thin Films Prepared by Atomic Layer Deposition. *J. Electrochem. Soc.* **1994**, *141*, 1278−1284.
(22) Pilvi, T.; Hatanpaa, T.; Puukilainen, E.; Arstila, K.; Bischoff, M.; Kaiser, U.; Kaiser, N.; Leskela, M.; Ritala, M. Study of a Novel ALD Process for Depositing MgF_2 Thin Films. *J. Mater. Chem.* **2007**, *17*, 5077−5083.
(23) Pilvi, T.; Puukilainen, E.; Kreissig, U.; Leskela, M.; Ritala, M. Atomic Layer Deposition of MgF_2 Thin Films Using TaF_5 as a Novel Fluorine Source. *Chem. Mater.* **2008**, *20*, 5023−5028.
(24) Pilvi, T.; Puukilainen, E.; Arstila, K.; Leskela, M.; Ritala, M. Atomic Layer Deposition of LaF_3 Thin Films Using $La(thd)_3$ and TiF_4 as Precursors. *Chem. Vap. Deposition* **2008**, *14*, 85−91.
(25) Pilvi, T.; Puukilainen, E.; Munnik, F.; Leskela, M.; Ritala, M. ALD of YF_3 Thin Films from TiF_4 and $Y(thd)_3$ Precursors. *Chem. Vap. Deposition* **2009**, *15*, 27−32.
(26) Mantymaki, M.; Hamalainen, J.; Puukilainen, E.; Munnik, F.; Ritala, M.; Leskela, M. Atomic Layer Deposition of LiF Thin Films from Li(thd) and TiF_4 Precursors. *Chem. Vap. Deposition* **2013**, *19*, 111−116.
(27) Hennessy, J.; Jewell, A. D.; Greer, F.; Lee, M. C.; Nikzad, S. Atomic Layer Deposition of Magnesium Fluoride via Bis-(ethylcyclopentadienyl)magnesium and Anhydrous Hydrogen Fluoride. *J. Vac. Sci. Technol., A* **2015**, *33*, 01A125.
(28) Putkonen, M.; Szeghalmi, A.; Pippel, E.; Knez, M. Atomic Layer Deposition of Metal Fluorides through Oxide Chemistry. *J. Mater. Chem.* **2011**, *21*, 14461−14465.
(29) Lee, Y.; Cavanagh, A. S.; George, S. M. *Atomic Layer Deposition of AlF_3 Using Trimethylaluminum and Hydrogen Fluoride-Pyridine*, 13th International Conference on Atomic Layer Deposition (ALD2013), San Diego, California, July 28−31, 2013.
(30) Lee, Y.; DuMont, J. W.; Cavanagh, A. S.; George, S. M. Atomic Layer Deposition of AlF_3 Using Trimethylaluminum and Hydrogen Fluoride. *J. Phys. Chem. C* **2015**, *119*, 14185−14194.
(31) Olah, G. A.; Nojima, M.; Kerekes, I. Synthetic Methods and Reactions 0.2. Hydrofluorination of Alkenes, Cyclopropane and Alkynes with (Trialkylamine) Reagents. *Synthesis* **1973**, *1973*, 779−780.
(32) Elam, J. W.; Groner, M. D.; George, S. M. Viscous Flow Reactor with Quartz Crystal Microbalance for Thin Film Growth by Atomic Layer Deposition. *Rev. Sci. Instrum.* **2002**, *73*, 2981−2987.
(33) Lee, Y.; Yoon, B.; Cavanagh, A. S.; George, S. M. Molecular Layer Deposition of Aluminum Alkoxide Polymer Films Using Trimethylaluminum and Glycidol. *Langmuir* **2011**, *27*, 15155−15164.
(34) Shannon, R. D.; Shannon, R. C.; Medenbach, O.; Fischer, R. X. Refractive Index and Dispersion of Fluorides and Oxides. *J. Phys. Chem. Ref. Data* **2002**, *31*, 931−970.
(35) Hausmann, D. M.; Kim, E.; Becker, J.; Gordon, R. G. Atomic Layer Deposition of Hafnium and Zirconium Oxides Using Metal Amide Precursors. *Chem. Mater.* **2002**, *14*, 4350−4358.
(36) *CRC Handbook of Chemistry and Physics*, 85th ed.; Lide, D. R., Ed., CRC Press: Boca Raton, FL, 2005.
(37) Almeida, R. M.; Morais, P. J. Preparation and Characterization of Amorphous ZrF_4 Thin Films. *J. Non-Cryst. Solids* **1995**, *184*, 93−97.
(38) Benjamin, S. L.; Levason, W.; Pugh, D.; Reid, G.; Zhang, W. J. Preparation and Structures of Coordination Complexes of the Very Hard Lewis Acids ZrF_4 and HfF_4. *Dalton Trans.* **2012**, *41*, 12548−12557.
(39) Burton, B. B.; Fabreguette, F. H.; George, S. M. Atomic Layer Deposition of MnO Using Bis(ethylcyclopentadienyl) Manganese and H_2O. *Thin Solid Films* **2009**, *517*, 5658−5665.
(40) Burton, B. B.; Goldstein, D. N.; George, S. M. Atomic Layer Deposition of MgO Using Bis(ethylcyclopentadienyl)magnesium and H_2O. *J. Phys. Chem. C* **2009**, *113*, 1939−1946.
(41) Kukli, K.; Ritala, M.; Leskela, M. Low Temperature Deposition of Zirconium Oxide-Based Nanocrystalline Films by Alternate Supply of $Zr[OC(CH_3)_3]_4$ and H_2O. *Chem. Vap. Deposition* **2000**, *6*, 297−302.
(42) Martin, P. M.; Olsen, L. C.; Johnston, J. W.; Depoy, D. M. Investigation of Sputtered HfF_4 Films and Application to Interference Filters for Thermophotovoltaics. *Thin Solid Films* **2002**, *420-421*, 8−12.
(43) Lee, Y.; Piper, D. M.; Cavanagh, A. S.; Young, M. J.; Lee, S.-H.; George, S. M. *Atomic Layer Deposition of Lithium Ion Conducting $(AlF_3)(LiF)_x$ Alloys Using Trimethylaluminum, Lithium Hexamethyldisilazide and Hydrogen Fluoride-Pyridine*, 14th International Conference on Atomic Layer Deposition (ALD2014), Kyoto, Japan, June 15−18, 2014.

DOI: 10.1021/acs.chemmater.5b04360
Chem. Mater. 2016, 28, 2022−2032

(44) Papiernik, R.; Mercurio, D.; Frit, B. The Structure of Zirconium Tetrafluoride, Alpha-ZrF_4. *Acta Crystallogr., Sect. B: Struct. Crystallogr. Cryst. Chem.* **1982**, *38*, 2347−2353.
(45) Srikharan, K.; Allen, T. R. *Chapter 12 on "Corrosion in Molten Salts" in Molten Salts Chemistry: From Lab to Applications*; Lantelme, F., Groult, H., Eds.; Elsevier, Inc.: Burlington, MA, 2013.
(46) Smith, D. W. An Acidity Scale for Binary Oxides. *J. Chem. Educ.* **1987**, *64*, 480−482.
(47) Kramer, G. M. Ranking Strong Acids via a Selectivity Parameter. 1. *J. Org. Chem.* **1975**, *40*, 298−302.
(48) Kramer, G. M. Ranking Strong Acids via a Selectivity Parameter. 2. *J. Org. Chem.* **1975**, *40*, 302−307.
(49) Wuttke, S.; Vimont, A.; Lavalley, J.-C.; Daturi, M.; Kemnitz, E. Infrared Investigation of the Acid and Basic Properties of a Sol-Gel Prepared MgF_2. *J. Phys. Chem. C* **2010**, *114*, 5113−5120.
(50) Guo, Y.; Wuttke, S.; Vimont, A.; Daturi, M.; Lavalley, J. C.; Teinz, K.; Kemnitz, E. Novel Sol-Gel Prepared Zinc Fluoride: Synthesis, Characterisation and Acid-Base Sites Analysis. *J. Mater. Chem.* **2012**, *22*, 14587−14593.
(51) Christe, K. O.; Dixon, D. A.; McLemore, D.; Wilson, W. W.; Sheehy, J. A.; Boatz, J. A. On a Quantitative Scale for Lewis Acidity and Recent Progress in Polynitrogen Chemistry. *J. Fluorine Chem.* **2000**, *101*, 151−153.
(52) Krahl, T.; Vimont, A.; Eltanany, G.; Daturi, M.; Kemnitz, E. Determination of the Acidity of High Surface AlF_3 by IR Spectroscopy of Adsorbed CO Probe Molecules. *J. Phys. Chem. C* **2007**, *111*, 18317−18325.
(53) Wander, A.; Bailey, C. L.; Searle, B. G.; Mukhopadhyay, S.; Harrison, N. M. Identification of Possible Lewis Acid Sites on the Beta-AlF_3(100) Surface: An ab initio Total Energy Study. *Phys. Chem. Chem. Phys.* **2005**, *7*, 3989−3993.
(54) Haupin, W. Chemical and Physical Properties of the Hall-Heroult Electrolyte. In *Molten Salt Chemistry: An Introduction and Selected Applications, NATO Science Series C*; Mamantov, G., Marassi, R., Eds.; D. Reidel Publishing Company: Dordrecht, Holland, 1987; Vol. *202*.
(55) Allen, T. H.; Lehan, J. P.; McIntyre, L. C., Jr. Ion Beam Sputtered Metal Fluorides. *Proc. SPIE* **1990**, 277−290.
(56) Waters, T. N. Some Investigations in the Zirconium Tetrafluoride-Water System. *J. Inorg. Nucl. Chem.* **1960**, *15*, 320−328.

DOI: 10.1021/acs.chemmater.5b04360
Chem. Mater. 2016, 28, 2022−2032